Soft Matter

PAPER

View Article Online
View Journal | View Issue

Cite this: *Soft Matter*, 2015, **11**, 3666

Complementary light scattering and synchrotron small-angle X-ray scattering studies of the micelle-to-unimer transition of polysulfobetaines†

Kay E. B. Doncom,[ab] Anaïs Pitto-Barry,[a] Helen Willcock,[a] Annhelen Lu,[a] Beulah E. McKenzie,[b] Nigel Kirby[c] and Rachel K. O'Reilly*[a]

Received 12th March 2015,
Accepted 19th March 2015

DOI: 10.1039/c5sm00602c

www.rsc.org/softmatter

AB and ABA di- and triblock copolymers where A is the hydrophilic poly(oligoethylene glycol methacrylate) (POEGMA) block and B is a thermo-responsive sulfobetaine block [2-(methacryloyloxy) ethyl] dimethyl-(3-sulfopropyl) ammonium hydroxide (PDMAPS) were synthesised by aqueous RAFT polymerisation with narrow dispersity ($Đ_M \leq 1.22$), as judged by aqueous SEC analysis. The di- and triblock copolymers self-assembled in salt-free water to form micelles with a PDMAPS core and the self-assembly of these polymers was explored by SLS and TEM analysis. The micelles were shown, by DLS analysis, to undergo a micelle-to-unimer transition at a critical temperature, which was dependent upon the length of the POEGMA block. Increasing the length of the third, POEGMA, block decreased the temperature at which the micelle-to-unimer transition occurred as a result of the increased hydrophilicity of the polymer. The dissociation of the micelles was further studied by SLS and synchrotron SAXS. SAXS analysis revealed that the micelle dissociation began at temperatures below that indicated by DLS analysis and that both micelles and unimers coexist. This highlights the importance of using multiple complementary techniques in the analysis of self-assembled structures. In addition the micelle-to-unimer morphology transition was employed to encapsulate and release a hydrophobic dye, Nile Red, as shown by fluorescence spectroscopy.

Introduction

Stimuli-responsive polymers are of great interest due to their ability to undergo a change in hydrophobicity in response to an external stimulus. One stimulus that has been widely investigated within the literature is temperature.[1–3] Thermo-responsive polymers can be divided into two classes, those which exhibit a lower critical solution temperature (LCST) and those which exhibit an upper critical solution temperature (UCST). LCST polymers have been widely studied and there are many examples of different polymers displaying LCST behaviour, with poly(*N*-isopropyl acrylamide) (PNIPAM) being one of the most widely studied.[1–6] In contrast, reports of polymers exhibiting UCST-type behaviour are far less common.[7,8] Indeed, in a recent review on thermo-responsive polymers, 57 examples of LCST type polymers were given, compared to just 5 displaying UCST behaviour.[3]

Polymeric betaines are a class of zwitterionic polymers in which the cationic and anionic functional groups are located on the same monomer unit.[9] Since their discovery in the 1950's these polymers are known to be salt-responsive and are often insoluble in pure water at room temperature but become soluble upon the addition of salt.[9–13] Betaines can also be categorised further into phosphobetaines,[14] carboxybetaines[15] and sulfobetaines,[13] which differ in the chemical nature of the groups which form the cationic and anionic functionalities. Not all sulfobetaines display UCST cloud points and of those that do, the cloud points have been found to be highly molecular weight and concentration dependent.[16–18] Sulfo- and phosphobetaines have also been reported to be biocompatible,[19–23] and exhibit reduced bacterial adhesion and protein fouling.[20]

Polymeric sulfobetaines can be synthesised in two ways, by direct polymerisation of a sulfobetaine monomer or polymerisation of the corresponding tertiary amino-methacrylate monomer and introduction of the sulfonate groups by post-polymerisation.[24–28] The advantage of the second method is the improved organic solubility of the precursor polymer, making chain extension and further polymer modifications simpler.

[a] *University of Warwick, Department of Chemistry, Gibbet Hill Road, Coventry, CV4 7AL, UK. E-mail: r.k.o-reilly@warwick.ac.uk; Tel: +44 (0)247 652 3236*
[b] *University of Sheffield, Department of Chemistry, Brook Hill, Sheffield, S3 7HF, UK*
[c] *Australian Synchrotron, 800 Blackburn Road, Clayton, Victoria 3168, Australia*

† Electronic supplementary information (ESI) available: DLS traces and count rate data, d*n*/d*c* calculations, further SAXS data, ^{1}H NMR data and fluorescence data. See DOI: 10.1039/c5sm00602c

Nevertheless, the post-polymerisation betainisation reaction requires the use of 1,3-propanesultone, which is extremely carcinogenic. Whilst the direct polymerisation of the sulfobetaine monomer eliminates this reaction step, the choice of polymerisation solvent is limited to water, salt solutions and some highly polar fluorinated solvents such as trifluoroethanol or hexafluoroisopropanol.[25–27]

Polymer molecular weight and molecular weight distribution can be controlled by using reversible deactivation radical (RDR) polymerisation techniques such as reversible addition-fragmentation chain-transfer (RAFT) polymerisation.[29] RAFT is arguably the most versatile RDR technique as it allows for the polymerisation of a wide range of monomers with various functionalities. Indeed, betaine monomers have been successfully polymerised by RAFT, yielding both homopolymers and block copolymers.[10,18,26,28,30–34]

To date there have been a limited number of examples of responsive multiblock copolymers containing sulfobetaines. One response that has been exploited is the superior solubility of polysulfobetaines in salt water compared to pure water.[11,12,30,31] For example, Donovan *et al.* prepared di- and triblock copolymers consisting of a sulfobetaine block, an *N*-methylacrylamide block and an *N*,*N*-dimethylacrylamide block and these polymers were found to transition between unimers and micelles with increasing or decreasing sodium chloride (NaCl) concentrations.[30] There have been fewer examples looking at temperature as a stimulus to induce a response in sulfobetaine-containing copolymers.[7,32,35–38] In one example, Che *et al.* synthesised copolymers of acrylamide and *N*,*N*′-dimethyl(methacryloylethyl) ammonium propane sulfonate (DMAPS) by free radical polymerisation. An increase in temperature caused the R_h of these polymers in water to increase, as determined by DLS analysis.[37] In another example Tian *et al.* synthesised a diblock copolymer consisting of POEGMA and a tertiary amine acrylamide monomer by RAFT polymerisation.[39] This polymer exhibited both LCST and UCST behaviour. The LCST cloud point could be tuned by incorporating varying amounts of 2-(2-methoxyethoxy) ethyl methacrylate into the POEGMA block. UCST behaviour was introduced by partial betainisation of the tertiary amine block with 1,3-propane sultone, and the degree of betainisation was shown to affect the UCST cloud point, as characterised by UV transmittance. Below the UCST of the betaine block aggregation was observed by light scattering, similarly for above the LCST cloud point of the PNIPAM block; however further characterisation of the solution self-assembly was not provided. Between these two temperatures the polymer was molecularly dissolved.

In this work we demonstrate precise control over the micelle-to-unimer transition temperature of sulfobetaine-containing block copolymers, achieved by altering the length of the hydrophilic POEGMA segments. To the best of the authors' knowledge this is the first example of triblock copolymers containing the sulfobetaine monomer DMAPS synthesised by RAFT polymerisation and the thorough characterisation of their self-assembly and thermo-responsive behaviour. The morphologies were extensively characterised using a combination of static light scattering (SLS) and dynamic light scattering (DLS). The transition between micelle and unimer was studied using synchrotron small-angle X-ray scattering (SAXS) and DLS, revealing that unimers are present before the transition is detected by light scattering. This highlights the need for complementary analysis when investigating the responsive properties of nanostructures. To demonstrate the utility of such nanostructures, the encapsulation and controlled release of a hydrophobic payload in response to a change in temperature is demonstrated.

Experimental

Materials

1,4-Dioxane, oligoethylene glycol methyl ether methacrylate (OEGMA), *N*,*N*′-dimethyl(methacryloylethyl) ammonium propane sulfonate (DMAPS), 4-cyano-4-(phenylcarbonothioylthio)-pentanoic acid (CTA 1) and 4,4′-azobis(4-cyanopentanoic acid) (ACVA) were used as received from Aldrich and Fluka. 2,2′-Azobis-(2-methylpropionitrile) (AIBN) was purchased from Molekula and recrystallised twice from methanol and stored in the dark at 4 °C.

Characterisation

Nuclear magnetic resonance (NMR) experiments were performed on a Bruker 400 FT-NMR spectrometer operating at 400 MHz (^{1}H) or 125 MHz (^{13}C) using deuterated water. Chemical shifts are reported in parts per million (ppm) relative to H_2O (4.79 ppm). Unless otherwise stated all spectra were obtained at 25 °C. Variable temperature ^{1}H NMR spectra were obtained on a 500 FT-NMR spectrometer operating at 500 MHz. Size exclusion chromatography (SEC) measurements were obtained in either HPLC grade DMF containing 0.1 M NH_4BF_4 at a flow rate of 1 mL min^{-1}, on a set of two Pgel 5 μm Mixed D columns plus a guard column, or in pH 8.2 phosphate buffer at a flow rate of 1 mL min^{-1}, on a set of one PL aquagel OH 50 column and one PL aquagel mixed M column plus a PL aquagel OH guard column. Cirrus SEC software was used to analyse the data using poly(methylmethacrylate) (PMMA) or poly(ethylene glycol) (PEG) standards.

Hydrodynamic diameters (D_h) and size distributions of the self-assembled structures in aqueous solutions were determined by DLS. The DLS instrumentation consisted of a Malvern ZetasizerNanoS instrument operating at 25 °C (unless otherwise stated) with a 4 mW He–Ne 633 nm laser module. Measurements were made at a detection angle of 173° (back scattering) and Malvern DTS 6.20 software was utilised to analyse the data. All measurements were run at least three times with a minimum of 10 runs per measurement.

SLS and DLS measurements were recorded simultaneously on an ALV CGS3 spectrometer consisting of a 22 mW HeNe laser at λ = 632.8 nm. Measurements were carried out at 20 °C, and recorded at least 7 scattering angles between 20 and 150°. The scattering vector was defined as

$$q = \frac{4\pi n}{\lambda}\sin\frac{\theta}{2}$$

where n is the refractive index (RI) of the solvent. Concentrations between 0.1 and 2 mg mL^{-1} were analysed for each sample. At least two measurements were run at each angle and each run for at least 100 seconds to determine the auto correlation function, $g_2(t)$, from DLS and the mean scattered intensity, I, from SLS. The dissolved polymers were found to exhibit two relaxation modes, as determined by analysing the correlation function achieved from multi-angle DLS. The two relaxation modes and their contribution to the total observed scattering were analysed and separated using REPES.[40] The concentration of the larger species contributing to the slow mode of relaxation was negligible and thus only scattering from the fast mode was used to determine the molecular weight M_w and the radius of gyration R_g. The inverse of the relaxation time for the fast mode divided by q^2 ($\tau_{fast}{}^{-1}/q^2$) was plotted against the scattering vector squared (q^2). This was extrapolated to zero angle and the intercept yields the apparent diffusion coefficient. The apparent diffusion coefficient ($D_{t,app}$) can be related to the relaxation time by $D_{t,app} = (q^2\tau)^{-1}$.

The apparent diffusion coefficients were then plotted against polymer concentration and extrapolated to zero concentration to give the translational diffusion coefficient. Using the Stokes–Einstein equation yields the hydrodynamic diameter.

$$D_h = \frac{k_B T}{3\pi\eta D_t}$$

In the above equation, D_h is the hydrodynamic diameter, k_B is the Boltzmann's constant, T is the temperature (in K), η is the viscosity of the solvent and D_t is the translational diffusion coefficient.

$Kc/R_{\theta,fast}$ *vs.* q^2 was plotted and from this the molecular weight and R_g for the nanostructures were determined. The aggregation number N_{agg} was determined by comparing the molecular weight of the assembled structures to the absolute molecular weight of the polymer (Fig. 2).

The differential refractive index (DRI) for the samples was calculated using a Shodex RI-101 refractometer. The refractive index response was plotted against concentration and the slope of the graph used to calculate the dn/dc using the following equation, where n° is the RI of the solvent and K is the instrument constant.

$$\frac{dn}{dc} = \frac{\text{slope} \times n^\circ}{K}$$

Transmission electron microscopy (TEM) characterisation was carried out using lacey carbon grids that had been treated with graphene oxide (GO). GO solutions were synthesised as previously described.[41] One drop of GO solution was deposited onto an argon plasma treated lacey carbon copper grid and left to air dry. 4 μL of 0.1 mg mL^{-1} solution was deposited onto the grid and blotted off after 30 seconds. Dry state TEM analysis was performed on a JEOL 2000FX microscope operating at 200 keV. For cryo-TEM sample vitrification was carried out on an automated vitrification robot (FEI Vitrobot Mark III) for plunging in liquid ethane. Cryo-TEM Cu 400 mesh lacey carbon grids (Agar scientific) were surface plasma treated using a Cressington 208 carbon coater prior to use. For vitrification, 7 μL of the polymer solution (5 mg mL^{-1} in water), equilibrated to 4 °C, was applied to the cryo-TEM grids inside the vitrobot chamber which was conditioned to 100% humidity and 4 °C. Cryo analysis was imaged on the FEI Tecnai G2 Spirit TEM. Number average particle diameters (D_{av}) were generated from the analysis of a minimum of 50 particles from at least three different micrographs. Fluorescence measurements were recorded on a Perkin Elmer LS 55 spectrometer. Dialysis tubing was purchased from Spectrum labs with molecular weight cut offs of 3.5 kDa and 12–14 kDa.

Small-angle X-ray scattering (SAXS) measurements were carried out on the SAXS/WAXS beam line at the Australian Synchrotron facility at a photon energy of 8.2 keV. The samples were prepared in 18.2 MΩ cm water and were run using 1.5 mm diameter quartz capillaries. Capillaries were held in a sample holder with temperature control achieved *via* a water bath connected to the sample holder. Temperatures of 5, 10, 19, 24, 28, 36, 40, and 50 °C were reached, and the sample was allowed to equilibrate at each temperature for 10 minutes. The measurements were collected at a sample to detector distance of 3.252 m to give a q range of 0.0015 to 0.07 $Å^{-1}$, where q is the scattering vector and is related to the scattering angle (2θ) and the photon wavelength (λ) by the following equation:

$$q = \frac{4\pi \sin(\theta)}{\lambda}$$

All patterns were normalised to fixed transmitted flux using a quantitative beam stop detector. The scattering from a blank (H_2O) was measured in the same location as sample collection and was subtracted for each measurement. The two-dimensional SAXS images were converted in one-dimensional SAXS profile ($I(q)$ *vs.* q) by circular averaging, where $I(q)$ is the scattering intensity. The functions used for the fitting from the NIST SANS analysis package were "Debye"[42] and "Core–Shell with Constant Core/Shell Ratio" models.[43] ScatterBrain[44] and Igor[45] software were used to plot and analyse data. The scattering length density of the solvent and the monomers were calculated using the "Scattering Length Density Calculator" provided by NIST Center for Neutron Research.[46] Limits for q range were applied for the fitting from 0.002 to 0.05 $Å^{-1}$. Scattering length densities used for the calculations are 1.02×10^{-5} $Å^{-2}$ (core), 1.04×10^{-5} $Å^{-2}$ (shell) and 9.46×10^{-6} $Å^{-2}$ (solvent).

Synthetic procedures

Synthesis of POEGMA homopolymer 1. OEGMA (average M_n 480 Da) (1 g, 2.1 mmol, 20 equiv.), CTA 1 (29 mg, 0.1 mmol, 1 equiv.) and AIBN (1.7 mg, 0.01 mmol, 0.1 equiv.) were dissolved in 1,4-dioxane (2 : 1 solvent : monomer) and placed in an oven-dried ampoule under nitrogen flow with a stirrer bar. The polymerisation mixture was degassed with at least three freeze–pump–thaw cycles, released to and sealed under nitrogen. The reaction was subsequently immersed in an oil bath at 65 °C for 6 hours. The polymer was purified by dialysis against nanopure water (18.2 MΩ cm) and recovered by lyophilisation yielding polymer **1** as a pink oil. M_n (^{1}H NMR) = 8.2 kDa,

M_n (DMF SEC, PMMA standards) = 10.1 kDa, $Đ_M$ = 1.08. ^{1}H NMR spectroscopy (400 MHz, D_2O): δ = 0.70–1.30 (m, 51H, $CH_2C(CH_3)$ of polymer backbone), 1.60–2.20 (m, 34H, $CH_2C(CH_3)$), 2.35–2.45 (m, 2H, CH_2CH_2COOH), 3.30–3.36 (s, 51H, OCH_3 of polymer side chain), 3.40–3.86 (m, 578H, CH_2CH_2O of polymer side chain), 4.20–4.40 (br s, 34H, $COOCH_2CH_2O$ of polymer side chain), 7.46–7.58 (m, 2H, Ar ring of CTA), 7.64–7.74 (m, 1H, Ar ring of CTA), 7.88–7.98 (m, 2H, Ar ring of CTA).

Synthesis of POEGMA-*b*-PDMAPS diblock 2. DMAPS (5 g, 18 mmol, 800 equiv.), homopolymer **1** (0.1 g, 0.02 mmol, 1 equiv.) and ACVA (1.2 mg, 0.005 mmol, 0.2 equiv.) were dissolved in 0.5 M NaCl solution (5 : 1 solvent : monomer) and placed in an oven-dried round-bottom flask under a flow of nitrogen with a stirrer bar. The solution was purged with nitrogen for 45 minutes and left under positive pressure of nitrogen. The polymerisation mixture was then heated at 65 °C for 6 hours. The polymer was purified by dialysis against 18.2 MΩ cm water and recovered by lyophilisation yielding polymer **2** as a pale pink solid. M_n (^{1}H NMR) = 209 kDa, M_n (Aqueous SEC, PEG standards) = 106.4 kDa, $Đ_M$ = 1.16, M_w (SLS) = 259 kDa. ^{1}H NMR spectroscopy (400 MHz, 0.5 M NaCl in D_2O): δ = 0.89–1.51 (m, 2211H, $CH_2C(CH_3)$ of polymer backbone), 1.60–2.60 (m, 1474H, $CH_2C(CH_3)$ of polymer backbone), 2.30–2.50 (br s, 1440H, $CH_2CH_2SO_3^-$ of DMAPS side chain), 3.05–3.15 (br s, 1440H, $CH_2CH_2SO_3^-$ of DMAPS side chain), 3.26–3.40 (br s, 4320H, $N^+(CH_3)_2$ of DMAPS side chain), 3.45–3.46 (s, 50H, OCH_3 of POEGMA side chain), 3.60–3.72 (br s, 1440H, $N^+(CH_3)_2CH_2$ of DMAPS side chain), 3.72–3.81 (br m, 600H, CH_2CH_2O of POEGMA side chain), 3.81–4.30 (br s, 1440H, OCH_2CH_2N of DMAPS side chain), 4.40–4.70 (br s, 1440H, OCH_2CH_2N of DMAPS side chain). ^{13}C NMR spectroscopy (500 MHz, 0.5M NaCl in D_2O): δ = 18.3, 18.5, 18.7, 44.8, 45.1, 47.5, 49.1, 49.3, 59.2, 62.0, 62.2, 63.4, 69.2, 69.7, 71.1, 177.5, 178.1, 221.7.

Synthesis of POEGMA-*b*-PDMAPS-*b*-POEGMA triblocks 3, 4 and 5. The general polymerisation technique for synthesis of the triblocks is detailed below. To achieve the different block lengths, the equivalents of OEGMA were altered. OEGMA (11 mg, 0.02 mmol, 20 equiv.), diblock copolymer **2** (0.25 g, 0.001 mmol, 1 equiv.) and ACVA (0.04 mg, 0.0002 mmol, 0.2 equiv.) were dissolved in 0.5 M NaCl (5 : 1 solvent : **2**) and placed in an oven-dried round-bottom flask with a stirrer bar. The solution was bubbled with nitrogen for 45 minutes and then placed in a preheated oil bath at 65 °C for 16 hours. The polymer was purified by dialysis and recovered by lyophilisation to yield the polymer as a very pale pink solid.

Polymer **3**, M_n (^{1}H NMR) = 211.9 kDa, M_n (Aqueous SEC, PEG standards) = 103.8 kDa, $Đ_M$ = 1.18, M_w (SLS) = 284 kDa. ^{1}H NMR spectroscopy (400 MHz, 0.5 M NaCl in D_2O): δ = 0.89–1.51 (m, 2230H, $CH_2C(CH_3)$ of polymer backbone), 1.60–2.60 (m, 1486H, $CH_2C(CH_3)$ of polymer backbone), 2.30–2.50 (br s, 1440H, $CH_2CH_2SO_3^-$ of DMAPS side chain), 3.05–3.15 (br s, 1440H, $CH_2CH_2SO_3^-$ of DMAPS side chain), 3.26–3.40 (br s, 4320H, $N^+(CH_3)_2$ of DMAPS side chain), 3.45–3.46 (s, 69H, OCH_3 of POEGMA side chain), 3.60–4.10 (m, 3660H, $N^+(CH_3)_2CH_2$ of DMAPS side chain, CH_2CH_2O of POEGMA side chain and OCH_2CH_2N of DMAPS side chain), 4.40–4.70 (br s, 1440H, OCH_2CH_2N of DMAPS side chain). ^{13}C NMR spectroscopy (125 MHz, 0.5 M NaCl in D_2O): δ = 18.3, 18.5, 18.7, 44.8, 45.1, 47.5, 49.1, 49.3, 51.5, 52.1, 54.2, 59.1, 62.2, 63.4, 69.5, 69.7, 71.1, 177.4, 178.1, 205.1.

Polymer **4**, M_n (^{1}H NMR) = 217.2 kDa, M_n (Aqueous SEC, PEG standards) = 101.2 kDa, $Đ_M$ = 1.20, M_w (SLS) = 317 kDa. ^{1}H NMR spectroscopy (400 MHz, 0.5 M NaCl in D_2O): δ = 0.89–2.60 (br m, 5260H, $CH_2C(CH_3)$ of polymer backbone, $CH_2C(CH_3)$ of polymer backbone, $CH_2CH_2SO_3^-$ of DMAPS side chain), 3.05–3.15 (br s, 1440H, $CH_2CH_2SO_3^-$ of DMAPS side chain), 3.26–3.40 (br s, 4320H, $N^+(CH_3)_2$ of DMAPS side chain), 3.45–3.46 (s, 100H, OCH_3 of POEGMA side chain), 3.60–4.10 (m, 4020H, $N^+(CH_3)_2CH_2$ of DMAPS side chain, CH_2CH_2O of POEGMA side chain and OCH_2CH_2N of DMAPS side chain), 4.40–4.70 (br s, 1440H, OCH_2CH_2N of DMAPS side chain). ^{13}C NMR spectroscopy (125 MHz, 0.5 M NaCl in D_2O): δ = 7.9, 18.3, 18.5, 18.7, 45.0, 45.1, 47.2, 47.5, 49.2, 51.5, 51.8, 52.1, 54.2, 58.2, 62.2, 63.4, 69.5, 69.7, 71.1, 130.1, 177.4, 178.0, 205.0, 232.5.

Polymer **5**, M_n (^{1}H NMR) = 225.8 kDa, M_n (Aqueous SEC, PEG standards) = 95.2 kDa, $Đ_M$ = 1.22, M_w (SLS) = 330 kDa. ^{1}H NMR spectroscopy (400 MHz, 0.5 M NaCl in D_2O): δ = 0.89–2.60 (br m, 5309H, $CH_2C(CH_3)$ of polymer backbone, $CH_2C(CH_3)$ of polymer backbone, $CH_2CH_2SO_3^-$ of DMAPS side chain), 3.05–3.15 (br s, 1440H, $CH_2CH_2SO_3^-$ of DMAPS side chain), 3.26–3.40 (br s, 4320H, $N^+(CH_3)_2$ of DMAPS side chain), 3.45–3.46 (s, 160H, OCH_3 of POEGMA side chain), 3.60–4.10 (m, 4660H, $N^+(CH_3)_2CH_2$ of DMAPS side chain, CH_2CH_2O of POEGMA side chain and OCH_2CH_2N of DMAPS side chain), 4.40–4.70 (br s, 1440H, OCH_2CH_2N of DMAPS side chain). ^{13}C NMR spectroscopy (125 MHz, 0.5 M NaCl in D_2O): δ = 18.3, 18.5, 18.7, 45.0, 45.1, 47.0, 47.3, 49.2, 51.5, 51.8, 52.1, 4.3, 58.2, 62.2, 63.4, 69.5, 69.7, 71.1, 130.1, 177.4, 178.0, 205.2, 232.4.

Self-assembly of the polymers. Polymers **2–5** were self-assembled by direct dissolution at 1 mg mL^{-1} in 18.2 MΩ cm water. The solutions were gently heated for a few minutes (*ca.* 40 °C) to aid dissolution and then were allowed to cool to room temperature with stirring to yield self-assembled structures **2′–5′**.

Encapsulation and release studies. The encapsulation and release studies were performed in the same manner for all self-assembled structures **2′–5′**. The polymer was self-assembled at a concentration of 1 mg mL^{-1}, then Nile Red was added until a concentration of 1 mg mL^{-1} was achieved. The solution was stirred overnight at 4 °C. Non-encapsulated Nile Red was removed by filtration through a 0.45 μm Nylon filter. The fluorescence response was then recorded by exciting at λ_{ex} 550 nm and recording the emission at 575 nm. The micelle solution was then heated (36 °C for **2′**, 38 °C for **3′**) for 5 minutes. The solution was then filtered whilst hot to remove the precipitated Nile Red and the fluorescence again recorded at λ_{ex} 550 nm with emission recorded at λ_{em} 575 nm.

Results and discussion

Synthesis of POEGMA-*b*-PDMAPS diblock copolymer, 2

The UCST behaviour of PDMAPS has previously been reported[16,37] which inspired our motivation to explore the effect of incorporating

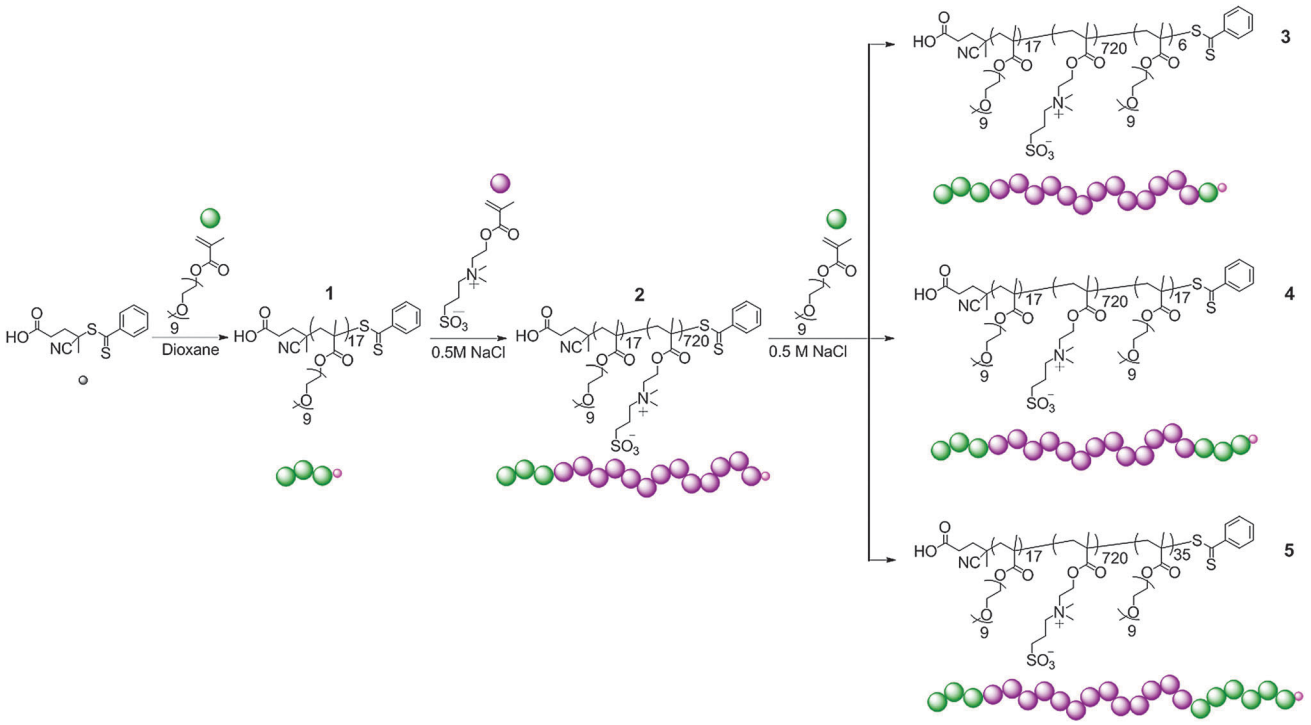

Scheme 1 The synthetic route to thermo-responsive diblock copolymer, **2**, and triblock copolymers, **3–5**.

a permanently hydrophilic block on the temperature response of PDMAPS using a variety of complimentary analytical techniques. RAFT techniques have previously been used to polymerise DMAPS, both as a homopolymer and as diblocks,[10,30,32–34] but the UCST behaviour of the diblock copolymers has not been fully explored.[32] To explore this phenomenon we designed a block copolymer with permanently hydrophilic OEGMA and temperature-responsive DMAPS segments (Scheme 1). To prepare this diblock copolymer, the permanently hydrophilic block was first synthesised from OEGMA, in 1,4-dioxane using 4-cyano-4-(phenylcarbonothioylthio)pentanoic acid as the chain transfer agent. After purification by dialysis (MWCO 12–14 kDa) and recovery by lyophilisation, the hydrophilic homopolymer **1** with $M_{n\,NMR}$ = 8.2 kDa $M_{n\,SEC}$ = 10.1 kDa and $Đ_M$ = 1.08 was isolated. The polymerisation proceeded with good control over molecular weight and molecular weight distribution, as shown by the low dispersity in SEC. The hydrophilic POEGMA was subsequently used as a macroCTA for the chain extension with DMAPS in 0.5 M NaCl yielding a responsive diblock copolymer, **2**, with $M_{n\,NMR}$ = 209 kDa, $M_{n\,SEC}$ = 106.4 kDa, $Đ_M$ = 1.16 (see Scheme 1). The dispersity after chain extension is within the range found in the literature for the RAFT polymerisation of DMAPS.[10,33,34,47,48] The block length of 720 units was targeted as it has previously been shown that homopolymers of DMAPS of a similar molecular weight display a UCST cloud point of *ca.* 26 °C at 1 mg mL^{-1}.[32]

Synthesis of triblock copolymers, 3–5

Triblock copolymers have been shown to self-assemble into interesting morphologies including cylindrical vesicles[49] and flower-like micelles.[30,50] The incorporation of sulfobetaines into amphiphilic triblock copolymers and the resulting self-assembly behaviour has not been thoroughly investigated within the literature. Of the examples of sulfobetaine-containing triblock copolymers, several utilise post-polymerisation modification techniques to introduce the betaine functionality, either by betainisation of the tertiary amine precursor[51] or by polymer–polymer coupling reactions.[52] In the previous examples, the thermo-response of the polymers was not reported. As a comparison to the diblock copolymer **2**, we report the synthesis of a series of triblock copolymers by chain-extending the diblock, **2**, with OEGMA to form ABA triblocks **3**, **4**, and **5** (see Scheme 1 and Table 1).

The length of the third block was calculated using ^{1}H NMR spectroscopy, by comparison of the POEGMA side chain signals in the triblock, **3**, **4** or **5**, to the starting diblock, **2**, using the betaine signals as a standard (Fig. 1).

Table 1 Molecular weight and dispersity of the diblock and triblock copolymers, calculated by ^{1}H NMR spectroscopy, aqueous SEC analysis and SLS analysis in 0.5 M NaCl solution[a]

	M_n, NMR (kDa)	M_n, SEC (kDa)	$Đ_M$	M_w, SLS (kDa)
2	209	106	1.16	259
3	212	104	1.18	284
4	217	101	1.20	317
5	226	95	1.22	330

[a] The molecular weight of the triblock polymers (**3–5**) as measured by SEC appears smaller than the diblock (**2**) due to increased interactions with the SEC column as the POEGMA block length increases. However, the molecular weight is shown to increase as expected by ^{1}H NMR and SLS.

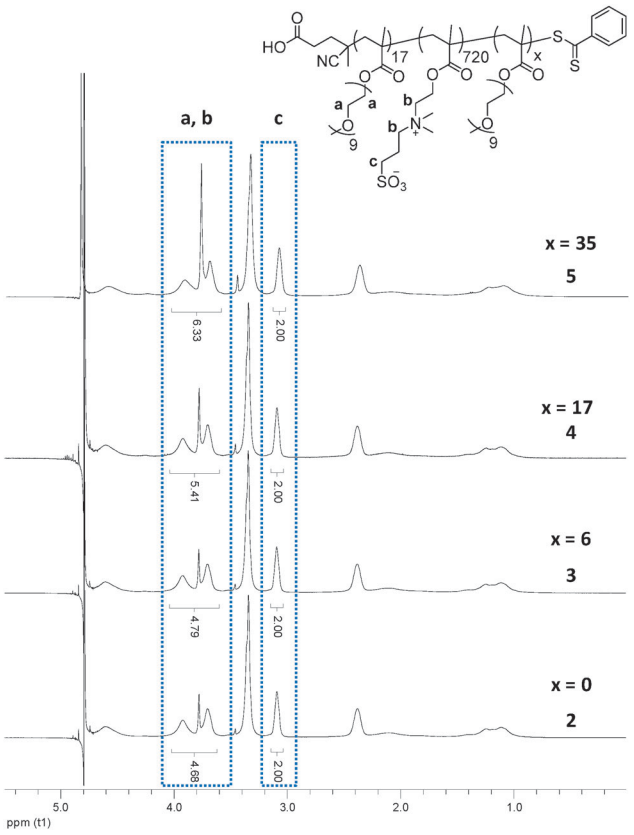

Fig. 1 ^{1}H NMR spectra (in 0.5 M NaCl in D_2O) showing the increase in the POEGMA length between polymers **2–5** at 20 °C.

Analysis of the di- and triblock copolymers 2–5 in 0.5 M NaCl solution by SLS

In order to obtain the absolute molecular weight the di- and triblock copolymers were analysed simultaneously by SLS and DLS in 0.5 M NaCl. The use of the salt solution ensured that the polymers remained in unimeric form and did not undergo aggregation or interaction. The dissolved polymers were found to exhibit two relaxation modes, as determined by analysing the correlation function achieved from multi-angle DLS. The two relaxation modes and their contribution to the total observed scattering were analysed and separated using REPES.[40]

The concentration of the larger species contributing to the slow mode of relaxation was attributed to slight particle aggregation, however this was determined to be negligible and thus only scattering from the fast mode was used to determine M_w and R_g. The Rayleigh ratio for the fast mode ($R_{\theta,\mathrm{fast}}$) was calculated as follows (eqn (1)):

$$R_{\theta,\mathrm{fast}} = A_{\mathrm{fast}}(q)R_{\theta} = \frac{A_{\mathrm{fast}}}{A_{\mathrm{fast}} + A_{\mathrm{slow}}}(q)\frac{I_{\mathrm{sample}}(q) - I_{\mathrm{solvent}}(q)}{I_{\mathrm{reference}}(q)}R_{\mathrm{reference}} \quad (1)$$

where $A_{\mathrm{fast}}(q)$ is the scattered intensity contribution at a given angle from the fast mode of relaxation as determined by DLS; I_{sample}, I_{solvent} and $I_{\mathrm{reference}}$ are the scattered intensities by the sample, the solvent and the reference respectively at a given angle, q, and $R_{\mathrm{reference}}$ is the Rayleigh ratio of the reference solvent, which in this case was toluene.

Concentrations between 0.5 and 2 mg mL^{-1} were measured at a minimum of 7 angles between 30 and 150°. The scattered intensity at each angle was measured for at least 100 s for each concentration and was then used to calculate the molecular weight (M_w) and radius of gyration (R_g) using eqn (2).

$$\frac{Kc}{R_{\theta,\mathrm{fast}}} = \frac{1}{M_w}\left(1 + \frac{q^2 {R_g}^2}{3}\right) + 2A_2c \quad (2)$$

where q is the scattering vector, A_2 is the second virial coefficient (related to polymer–polymer and polymer–solvent interactions), c is the polymer concentration, K is a constant calculated according to eqn (3) and $R_{\theta,\mathrm{fast}}$ is the Rayleigh ratio of the fast mode of the sample calculated using eqn (1).

$$K = \frac{4\pi^2 {n_{\mathrm{ref}}}^2 \left(\frac{\mathrm{d}n}{\mathrm{d}c}\right)^2}{\lambda^4 N_A} \quad (3)$$

where n_{ref} is the refractive index of the reference (toluene), dn/dc is the calculated refractive index increment of the polymer solution, λ is the wavelength of the laser (=632.8 nm) and N_A is Avogadro's number. $Kc/R_{\theta,\mathrm{fast}}$ was plotted against q^2 for each concentration and each plot was extrapolated to zero q. The extrapolated $Kc/R_{\theta,\mathrm{fast}}$ was subsequently plotted against polymer concentration (Fig. 2). The line was extrapolated to zero concentration and the inverse of the intercept yielded the absolute molecular weight. The second virial coefficient (A_2) is determined from the gradient of this line and describes the interactions between polymer and solvent. For polymer **2** the molecular weight was determined to be 259 kDa. The triblock copolymers were also analysed in a similar manner and the molecular weights calculated. For triblock copolymer **3** the molecular weight was determined to be 284 kDa and the molecular weights of **4** and **5** were found to be 317 kDa and 330 kDa, respectively (Table 1). For all polymers **2–5** A_2 is positive, meaning that the polymer–solvent interactions are stronger than polymer–polymer interactions and indicates 0.5 M NaCl solution

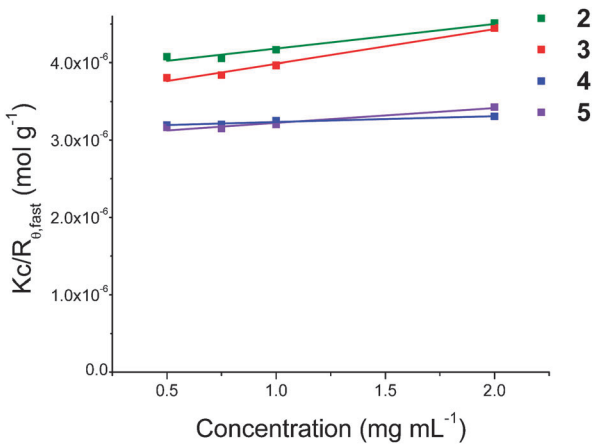

Fig. 2 Plot of $Kc/R_{\theta,\mathrm{fast}}$ *vs.* concentration for **2–5** in salt solution at 20 °C. The M_w was calculated using the intercept of the linear fit to the SLS data.

is a good solvent for the polymers and aggregation does not occur. The angular dependence of the dissolved polymers in 0.5 M NaCl solution was investigated by plotting the inverse of the relaxation time for the fast mode divided by q^2 ($\tau_{fast}{}^{-1}/q^2$) against the scattering vector squared (q^2). This showed that the polymer chains scatter isotropically and therefore are suitable for analysis by SLS (see ESI†).

Self-assembly of polymers 2–5

Block copolymer **2** was self-assembled by direct dissolution into 18.2 MΩ cm water at 1 mg mL^{-1}, with gentle heating to aid polymer dissolution and then left to stir at room temperature to give **2′**. Analysis by DLS of **2′** gave a single population with a D_h of 74 ± 2 nm. Spherical micellar structures with an average diameter of 65 ± 8 nm were observed by dry state TEM analysis of a solution of **2′** at 0.1 mg mL^{-1} deposited on a graphene oxide support (see Fig. 3). The smaller size observed in TEM is a result of drying effects.[53] The somewhat unexpected assembly of the polymers into core–shell micelles rather than vesicles is explained in the following sections and in Fig. S9 (ESI†).

Triblock copolymers **3**, **4**, and **5** were also self-assembled in a similar manner to form **3′**, **4′**, and **5′**. The self-assembled solutions were analysed by DLS and the sizes found to be similar to **2′** (Table 2). TEM analysis of these self-assembled structures proved challenging as the particles dissociated on the TEM grid during the drying process. This is a result of the polysulfobetaine core retaining significant hydrophilicity below T_{trans} (see ESI† for discussion). This effect is increased from **2′** to **3′**–**5′** due to the presence of the second POEGMA block in **3′**, **4′**, and **5′**. Therefore self-assembled solution **3′** was analysed by cryo-TEM (thereby avoiding the drying process) and micelles with a D_h = 69 ± 7 nm were observed (Fig. 4). This correlates well with the size observed by DLS (Table 2).

DLS and SLS analysis of the self-assembled structures 2′–5′ in water

The absolute M_w of the self-assembled structures, **2′**, in 18.2 MΩ cm water was determined to be 28 MDa, in the same manner as described previously for the dissolved polymers **2**–**5**. This corresponds to a N_{agg} of 103 polymer chains per micelle, using an absolute M_w for an individual polymer chain of 259 kDa.

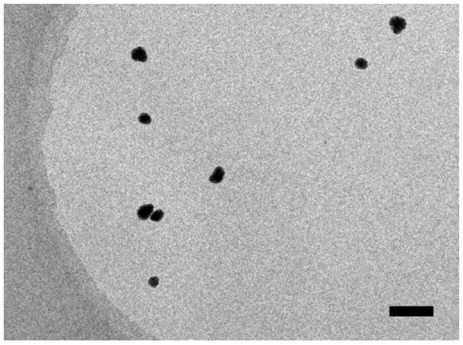

Fig. 3 Dry state TEM image of micelles **2′**, at 0.1 mg mL^{-1}, imaged on a graphene oxide support,[54] scale bar = 200 nm.

Table 2 Summary of the analysis of the self-assembled solutions **2′**–**5′** by multi-angle DLS and SLS

	N_{agg}	R_g (nm)	R_h (nm)	R_g/R_h [a]	T_{trans} (°C)
2′	103	37	45	0.84	34
3′	86	28	37	0.75	36
4′	77	31	37	0.84	32
5′	54	27	37	0.73	28

[a] Measured at 1 mg mL^{-1}.

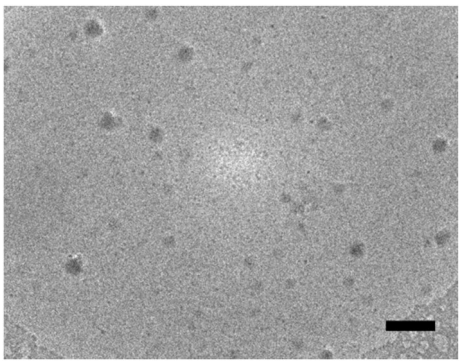

Fig. 4 Cryo-TEM image of micelles **3′** at 5 mg mL^{-1}, scale bar = 200 nm.

The self-assembled solutions **3′**–**5′** were also analysed by DLS and SLS at 20 °C and the results shown in Table 2. Plotting the inverse of the relaxation time for the fast mode divided by q^2 ($\tau_{fast}{}^{-1}/q^2$) against the scattering vector squared (q^2) showed that there was no significant angular dependence of the self-assembled particles (see ESI†) meaning that the particles scatter isotropically and therefore reliable R_h can be obtained. The R_g/R_h at 1 mg mL^{-1} for all polymers is between 0.73–0.84, suggesting that the self-assembled structures are micelles, rather than vesicles.[55] The M_w of the micelles, the aggregation number and the transition temperature decrease as the overall hydrophilicity of the polymer (governed by the length of the additional POEGMA block) increases (Table 2).

The second virial coefficient (A_2) for the self-assembled polymers in water were positive, meaning that water is a good solvent for the assembles and aggregation does not occur (see ESI† for further discussion).

Thermo-responsive properties of 2′–5′

As PDMAPS has been shown to display UCST behaviour, the self-assembled solution **2′** was heated in the DLS instrument and the size measured every 2 °C from 4 to 50 °C, with 5 minutes of equilibration at each temperature. The obvious dissociation of the self-assembled structures occurs at *ca.* 34 °C (Fig. 5).

The same heating procedure was performed on a solution of diblock copolymer **2** in 0.5 M NaCl solution at 1 mg mL^{-1}. In this case, no self-assembled structures are observed across the whole temperature range, which shows that as expected the salt suppresses the UCST behaviour of the DMAPS block. SAXS, like SLS or DLS, provides information on the entire solution, which is not the case for TEM. Moreover SAXS allows access to

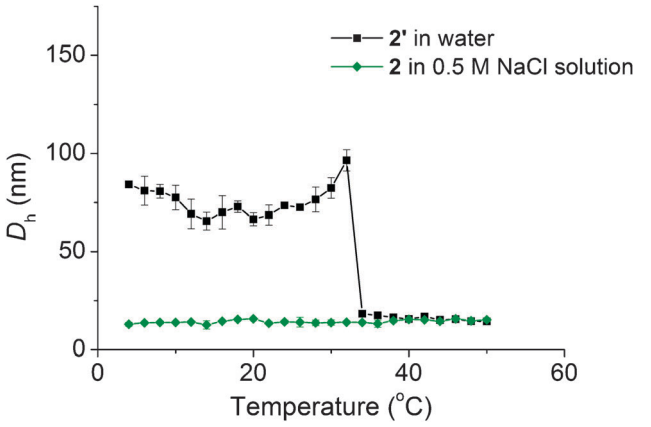

Fig. 5 Plot showing the change in D_h with temperature for diblock copolymer **2′** at 1 mg mL^{-1} in water and **2** at 1 mg mL^{-1} in 0.5 M NaCl solution.

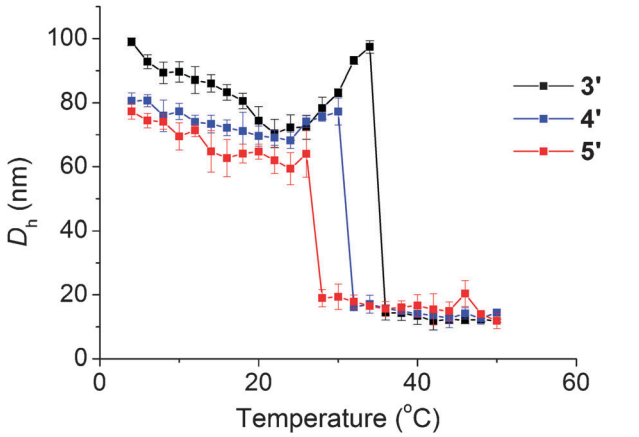

Fig. 6 Variable temperature DLS results (D_h) showing how the transition temperature for **3′**, **4′**, and **5′** decreases as the length of the third block increases.

complementary information, as modelling can be done to provide the shape and dimensions of the objects in solution. Variable temperature SAXS studies were performed in order to confirm the morphology of the diblock copolymer **2** between 5 and 50 °C (see Fig. S6 and Table S4, ESI†). At temperatures up to 10 °C a core–shell spherical micelle model was found to fit well, which provides the dimensions of the assembly with a core radius of 17–20 nm and a hydrated shell thickness of 6–10 nm. At 40 °C and above, a unimer model was found to fit well, with an R_g of *ca.* 11 nm. Between 19 and 32 °C, a linear combination of these two models accounted for the coexistence of both unimers and micelles. Moreover, by assuming that the spherical micelles were hard spheres with no solvent inside, the number of micelles per total volume was calculated and found to follow a decreasing trend as temperature increased. The volume fraction of unimers increases significantly at 36 °C, which is close to the temperature at which the micelle-to-unimer transition is observed by DLS analysis (34 °C).

The observation of unimers at temperatures below the dissociation temperature (calculated from DLS analysis) shows that some unimer exchange is occurring, and it is interesting to note that the unimers below the dissociation temperature are not detected in the DLS size distributions. However, analysis of the DLS count rate data shows a gradual decrease in intensity, not a sudden drop at the transition temperature, as would be expected for a dramatic morphology change (Fig. S7, ESI†). This highlights that the use of SAXS gives a much more detailed account of the true nature of the solution state of the polymers through this transition in morphology.

The temperature dependent assembly/disassembly of the triblock self-assembled solutions **3′**, **4′**, and **5′** were also investigated using DLS analysis as described for **2′**. A solution of polymer (1 mg mL^{-1}) was heated from 4 °C to 50 °C with measurements being taken every 2 °C and for each solution a clear micelle-to-unimer transition was observed. The temperature at which the transition occurred (T_{trans}) varied between the triblocks. **3′**, formed from triblock **3** that bears the shortest hydrophilic third block, showed a slight increase in the transition temperature (at 36 °C) as compared to **2′** (at 34 °C). This could be a result of a slight difference in packing between the diblock and the triblock copolymers. However, micelles formed from **4** (**4′**) displayed a transition temperature of 32 °C whilst those with the longest length hydrophilic third block, **5′**, underwent a morphology transition at 28 °C (Fig. 6).

This trend of a decrease in the transition temperature as the length of the third block increases can be explained by the increase in the overall hydrophilicity of the polymer. This higher level of hydrophilicity means that the dissociation temperature (at which the central DMAPS block is hydrophilic enough to cause dissolution into unimers) is lower. This demonstrates that the temperature at which the morphology transition occurs can easily be tailored by modifying the length of the DMAPS block.

Variable temperature SAXS studies were performed on self-assembled solution **3′** and similar results to **2′** were observed. At temperatures up to 10 °C a core–shell spherical micelle model was found to fit well. At 36 °C and above, a unimer model was found to fit well (Fig. 7).

Between 19 and 32 °C, a linear combination of these two models accounted for the coexistence of both unimers and micelles, with an increase in the unimer/micelle volume fraction ratio with increasing temperature (Table 3). The volume fraction of unimers increases significantly at 36 °C, the temperature at which the micelle-to-unimer transition is observed by DLS analysis.

Again, this mixture of unimers and micelles below the dissociation temperature is not observable by DLS size distribution analysis, although again the count rate data shows a gradual decrease (Fig. S7, ESI†). The presence of solely unimers at 40 °C and above correlates well with the results from DLS analysis. The shell thickness observed for **3′** (9 ± 1 nm at 5 °C) is thicker than that seen in **2′** (from 6 ± 1 nm at 5 °C) while a decrease of the core radius is also observable (from 20 ± 1 nm in **2′** to 15 ± 1 nm in **3′** at 5 °C).

The increase in the thickness of the shell can be explained by the presence of the third, hydrophilic POEGMA, block.

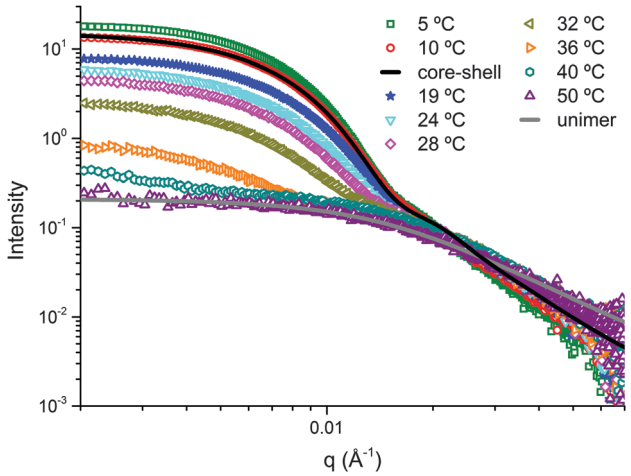

Fig. 7 SAXS profiles for **3′** in water at different temperatures between 10 °C and 50 °C with core–shell and unimer model fits shown in solid lines.

The decrease in the core radius upon going from the diblock to the triblock can be explained by better packing in the ABA triblock, or by the higher hydrophilicity of the triblock. The incorporation of a hydrophilic monomer into homopolymers of DMAPS has been shown to decrease the cloud point of the polymer and therefore the presence of this second hydrophilic block could cause the DMAPS block to be more hydrophilic in the triblock than in the diblock at 20 °C.[32] Indeed, the formation of core–shell micelles for all polymers is somewhat unexpected, as based on the short block length of the hydrophilic POEGMA and the much longer responsive betaine block, a vesicle-type structure is expected.[56–59]

To try to explain the unexpected assembly behaviour of the diblock variable temperature ^{1}H NMR spectroscopy studies were performed on **3′** to monitor the change in hydrophobicity of the PDMAPS block with changing temperature. The results suggest that 30% of PDMAPS hydrophilicity is still retained at a temperature as low as 5 °C (Fig. S9, ESI†) indicating that the PDMAPS does not undergo a complete transformation to a fully hydrophobic polymer. This, combined with the calculation of the hydrophilic volume fraction of the diblock copolymer explains the unexpected self-assembly behaviour. The density of a DMAPS homopolymer of a similar molecular weight (200 kDa) was measured to be 1.06 g mL^{-1} and if the entirety of the DMAPS block was fully hydrophobic, the hydrophilic volume fraction of the diblock copolymer **3** is only 3.75%. However, based on the ^{1}H NMR data which suggests that 30% of the DMAPS block retains its hydrophilicity, the hydrophilic volume fraction of the polymer is 37%, a ratio that would normally result in micelle formation. Therefore the hydrophobic : hydrophilic ratio of the polymer is not directly proportional to the block lengths of the POEGMA and PDMAPS and the amphiphilic balance is not as expected, rationalising the formation of micelles rather than vesicles. This highlights the complexity of PDMAPS as a responsive polymer and the challenges in interpreting its thermo-responsive and self-assembly behaviour.

Encapsulation and release

The micelle-to-unimer transition in this system can be utilised to encapsulate and release hydrophobic cargo in response to temperature. To test this, Nile Red (a hydrophobic dye) was encapsulated into the micelles **2′** by simply stirring, at 1 mg mL^{-1}, in a 1 mg mL^{-1} polymer micelle aqueous solution overnight. Excess Nile Red was removed by filtering through a 0.45 μm filter. The fluorescence of the micelle solution was monitored (λ_{ex} = 550 nm and λ_{em} = 575 nm). To release the dye the micelle solution was heated at 36 °C for 5 minutes. The hot solution was then filtered to remove the released dye that had precipitated and again the fluorescence response of the solution was measured. After this procedure a much reduced fluorescence response from the nanostructure was observed (Fig. 8).

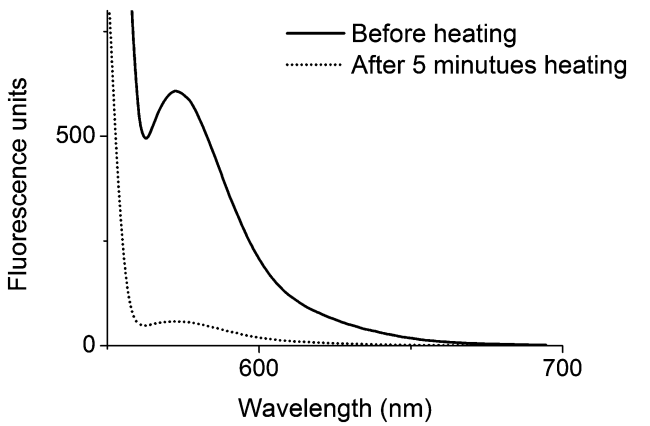

Fig. 8 Fluorescence spectra (λ_{ex} = 500 nm) showing the decrease in fluorescence after heating the micelle solution of **2′**.

Table 3 Showing the morphologies present at each temperature and the ratio of micelles to unimers, for **3′** as calculated by SAXS analysis

Temp. (°C)	Morphology (ratio micelle : unimer)	Vol. fraction (ratio micelle : unimer ×10^4)	No. of micelles (a.u.)
10	Micelles	20 : 0	401
19	Micelles and unimers	1 : 311	145
24	Micelles and unimers	1 : 687	72
28	Micelles and unimers	1 : 1141	41
32	Micelles and unimers	1 : 1197	19
36	Micelles and unimers	1 : 7583	12
40	Unimers	0 : 2729	0
50	Unimers	0 : 2088	0

The color change of the solution, from purple to colorless upon heating, was also easily observed. To confirm that the decrease in fluorescence was not a result of the filtration process, a non-heated micelle sample was filtered multiple times and no significant decrease in fluorescence was observed (Fig. S10, ESI†). Similar results were observed for the triblock copolymers (Fig. S11, ESI†).

Conclusions

In this report we have successfully synthesised diblock and triblock copolymers containing a thermo-responsive polysulfobetaine block by aqueous RAFT polymerisation. The assembly of these copolymers yielded well-defined spherical micelles with a PDMAPS core, which was unexpected given the hydrophobic weight fractions of the copolymers.

The self-assembled structures were analysed by SLS and synchrotron SAXS to confirm the formation of micelles and variable temperature ^{1}H NMR spectroscopy was used in order to understand the unusual morphology adopted for these block ratios. It was observed that even at temperatures well below the UCST cloud point of the DMAPS block, the polymer retained a significant degree of hydrophilicity, which may explain the unexpected morphology adopted. All of the micelle systems were shown to display UCST behaviour and their thermo-responsive behaviour was investigated by DLS analysis. All were observed to undergo a micelle-to-unimer morphology transition. This morphology transition was exploited to encapsulate the hydrophobic dye, Nile Red, within the micelles and release it upon heating. The speed of the release is fast and it is possible to tailor the temperature at which the micelle-to-unimer transition occurs by altering the length of the hydrophilic block. Both DLS and SAXS were used to probe the thermo-responsive behaviour of the micelles. Whilst DLS indicated that there was only one population below the transition temperature, *in situ* SAXS revealed the presence of two populations consisting of varying ratios micelles and unimers close to the transition temperature. Both techniques confirmed the sole presence of unimers at higher temperatures. These results highlight the importance of using multiple, complementary, techniques in order to fully evaluate the behaviour of such responsive self-assembled systems.

Acknowledgements

The authors would like to thanks the EPSRC and the University of Warwick Postgraduate Research Scholarship for funding. The University of Warwick Research Development Fund and the Swiss National Science Foundation are also acknowledged for financial support. Miss Dafni Moatsou is acknowledged for supplying part of the TOC graphic.

Notes and references

1 F. D. Jochum and P. Theato, *Chem. Soc. Rev.*, 2013, **42**, 7468.
2 M. I. Gibson and R. K. O'Reilly, *Chem. Soc. Rev.*, 2013, **42**, 7204.
3 D. Roy, W. L. A. Brooks and B. S. Sumerlin, *Chem. Soc. Rev.*, 2013, **42**, 7214.
4 L. Klouda and A. G. Mikos, *Eur. J. Pharm. Biopharm.*, 2008, **68**, 34.
5 R. Liu, M. Fraylich and B. Saunders, *Colloid Polym. Sci.*, 2009, **287**, 627.
6 S. Dai, P. Ravi and K. C. Tam, *Soft Matter*, 2009, **5**, 2513.
7 J. Seuring and S. Agarwal, *Macromol. Rapid Commun.*, 2012, **33**, 1898.
8 J. Seuring and S. Agarwal, *ACS Macro Lett.*, 2013, **2**, 597.
9 A. B. Lowe and C. L. McCormick, *Chem. Rev.*, 2002, **102**, 4177.
10 B. Yu, A. B. Lowe and K. Ishihara, *Biomacromolecules*, 2009, **10**, 950.
11 J. C. Salamone, W. Volksen, A. P. Olson and S. C. Israel, *Polymer*, 1978, **19**, 1157.
12 V. M. Monroy Soto and J. C. Galin, *Polymer*, 1984, **25**, 121.
13 R. Hart and D. Timmerman, *J. Polym. Sci.*, 1958, **28**, 638.
14 S. Nakai, T. Nakaya and M. Imoto, *Makromol. Chem.*, 1977, **178**, 2963.
15 H. Ladenheim and H. Morawetz, *J. Polym. Sci.*, 1957, **26**, 251.
16 D. N. Schulz, D. G. Peiffer, P. K. Agarwal, J. Larabee, J. J. Kaladas, L. Soni, B. Handwerker and R. T. Garner, *Polymer*, 1986, **27**, 1734.
17 M. Noh, Y. Mok, D. Nakayama, S. Jang, S. Lee, T. Kim and Y. Lee, *Polymer*, 2013, **54**, 5338.
18 M. Arotçaréna, B. Heise, S. Ishaya and A. Laschewsky, *J. Am. Chem. Soc.*, 2002, **124**, 3787.
19 Y. J. Shih, Y. Chang, A. Deratani and D. Quemener, *Biomacromolecules*, 2012, **13**, 2849.
20 S. L. West, J. P. Salvage, E. J. Lobb, S. P. Armes, N. C. Billingham, A. L. Lewis, G. W. Hanlon and A. W. Lloyd, *Biomaterials*, 2004, **25**, 1195.
21 Y. Chang, S. C. Liao, A. Higuchi, R. C. Ruaan, C. W. Chu and W. Y. Chen, *Langmuir*, 2008, **24**, 5453.
22 Y. Chang, S. H. Shu, Y. J. Shih, C. W. Chu, R. C. Ruaan and W. Y. Chen, *Langmuir*, 2009, **26**, 3522.
23 Y. J. Shih and Y. Chang, *Langmuir*, 2010, **26**, 17286.
24 V. Butun, C. E. Bennett, M. Vamvakaki, A. B. Lowe, N. C. Billingham and S. P. Armes, *J. Mater. Chem.*, 1997, **7**, 1693.
25 A. B. Lowe, N. C. Billingham and S. P. Armes, *Chem. Commun.*, 1996, 1555.
26 A. B. Lowe, N. C. Billingham and S. P. Armes, *Macromolecules*, 1999, **32**, 2141.
27 M. B. Huglin and M. A. Radwan, *Makromol. Chem.*, 1991, **192**, 2433.
28 Z. Tuzar, H. Pospisil, J. Plestil, A. B. Lowe, F. L. Baines, N. C. Billingham and S. P. Armes, *Macromolecules*, 1997, **30**, 2509.
29 G. Moad, E. Rizzardo and S. H. Thang, *Polymer*, 2008, **49**, 1079.
30 M. S. Donovan, A. B. Lowe, T. A. Sanford and C. L. McCormick, *J. Polym. Sci., Part A: Polym. Chem.*, 2003, **41**, 1262.
31 D. Wang, T. Wu, X. Wan, X. Wang and S. Liu, *Langmuir*, 2007, **23**, 11866.

32 H. Willcock, A. Lu, C. F. Hansell, E. Chapman, I. R. Collins and R. K. O'Reilly, *Polym. Chem.*, 2014, **5**, 1023.
33 C. L. McCormick and A. B. Lowe, *Acc. Chem. Res.*, 2004, **37**, 312.
34 H. Wang, T. Hirano, M. Seno and T. Sato, *Eur. Polym. J.*, 2003, **39**, 2107.
35 P. Mary, D. D. Bendejacq, M. P. Labeau and P. Dupuis, *J. Phys. Chem. B*, 2007, **111**, 7767.
36 P. A. Woodfield, Y. Zhu, Y. Pei and P. J. Roth, *Macromolecules*, 2014, **47**, 750.
37 Y. J. Che, Y. Tan, J. Cao and G. Y. Xu, *J. Macromol. Sci., Part B: Phys.*, 2010, **49**, 695.
38 J. Virtanen, M. Arotçaréna, B. Heise, S. Ishaya, A. Laschewsky and H. Tenhu, *Langmuir*, 2002, **18**, 5360.
39 H.-Y. Tian, J.-J. Yan, D. Wang, C. Gu, Y.-Z. You and X.-S. Chen, *Macromol. Rapid Commun.*, 2011, **32**, 660.
40 J. Jakes, *Collect. Czech. Chem. Commun.*, 1995, **60**, 1781.
41 N. R. Wilson, P. A. Pandey, R. Beanland, R. J. Young, I. A. Kinloch, L. Gong, Z. Liu, K. Suenaga, J. P. Rourke, S. J. York and J. Sloan, *ACS Nano*, 2009, **3**, 2547.
42 R. J. Roe, *Methods of X-ray and Neutron Scattering in Polymer Science*, Oxford University Press, 2000.
43 J. B. Hayter, in *Physics of Amphiphiles-Micelles, Vesicles, and Microemulsions*, ed. V. M. C. DeGiorgio, North-Holland Publishing Company, 1983, p. 59.
44 S. T. Mudie, *1.15 ed. Australian Synchrotron*, 2013.
45 S. Kline, *J. Appl. Crystallogr.*, 2006, **39**, 895–900.
46 NIST SLD calculator, http://www.ncnr.nist.gov/resources/sldcalc.html.
47 M. S. Donovan, B. S. Sumerlin, A. B. Lowe and C. L. McCormick, *Macromolecules*, 2002, **35**, 8663.
48 C. L. McCormick and A. B. Lowe, *Acc. Chem. Res.*, 2004, **37**, 312.
49 M. J. Barthel, U. Mansfeld, S. Hoeppener, J. A. Czaplewska, F. H. Schacher and U. S. Schubert, *Soft Matter*, 2013, **9**, 3509.
50 F. Huo, C. Gao, M. Dan, X. Xiao, Y. Su and W. Zhang, *Polym. Chem.*, 2014, **5**, 2736.
51 T. Wu, D. Wang, M. Zhang, J. R. Heflin, R. B. Moore and T. E. Long, *ACS Appl. Mater. Interfaces*, 2012, **4**, 6552.
52 S. Zhai, Y. Ma, Y. Chen, D. Li, J. Cao, Y. Liu, M. Cai, X. Xie, Y. Chen and X. Luo, *Polym. Chem.*, 2014, **5**, 1285.
53 J. P. Patterson, M. P. Robin, C. Chassenieux, O. Colombani and R. K. O'Reilly, *Chem. Soc. Rev.*, 2014, **43**, 2412.
54 J. P. Patterson, A. M. Sanchez, N. Petzetakis, T. P. Smart, T. H. Epps III, I. Portman, N. R. Wilson and R. K. O'Reilly, *Soft Matter*, 2012, **8**, 3322.
55 W. Burchard, *Light Scattering from Polymers*, Springer, Berlin, Heidelberg, 1983, vol. 48, p. 1.
56 A. Blanazs, S. P. Armes and A. J. Ryan, *Macromol. Rapid Commun.*, 2009, **30**, 267.
57 A. A. Choucair, A. H. Kycia and A. Eisenberg, *Langmuir*, 2003, **19**, 1001.
58 D. J. Adams, M. F. Butler and A. C. Weaver, *Langmuir*, 2006, **22**, 4534.
59 T. Azzam and A. Eisenberg, *Angew. Chem., Int. Ed.*, 2006, **45**, 7443.

